Results in Surfaces and Interfaces 4 (2021) 100018

Contents lists available at ScienceDirect

Results in Surfaces and Interfaces

journal homepage: www.elsevier.com/locate/rsurfi

Electroanalytical and surface studies on the protective action of a coating of PVA@3WGO on mild steel in acidic and saline environment

Anila Paul, Shamsheera K.O., Anupama R. Prasad, Abraham Joseph *

Department of Chemistry, University of Calicut, Calicut University P O, Kerala, India

ARTICLE INFO

Keywords:
Graphene oxide
PVA
Mild steel corrosion
FESEM
AFM

ABSTRACT

Corrosion aversion capability of Polyvinyl alcohol (PVA) coatings with different loading levels of Graphene Oxide (GO) nanoparticles on mild steel testing panels has been studied in different aggressive media. The chemical structure of the developed coatings was studied by FTIR, UV–Visible, and X-ray diffraction studies. The viability of the coating to offer corrosion resistance and the barrier performance were investigated by potentiodynamic polarization and electrochemical impedance spectroscopy. The surface morphology of the material was characterized by FESEM and AFM techniques. The electrochemical and non-electrochemical corrosion study of the coated panels were compared with uncoated mild steel panel and showed that PVA polymer matrix filled with 3.0 weight % of GO (PVA@3WGO) gives better protection in 0.5M HCl and 3.5% NaCl.

1. Introduction

Since mild steel (MS) as low carbon constituent steel, has an extensive range of applications varying from agricultural to the industrial sector mainly due to its affordability, weldability, and machinability. According to the "International Measures of Prevention, Application, and Economics of Corrosion Technology (IMPACT)" studies, the global cost of corrosion is estimated to be 3.4% of the global gross domestic product (GDP). So, it is very relevant that implementing corrosion prevention best practices could result in global savings of between 15%–35% of the cost of damage (Kroon et al., 2019). Since MS does not contain the alloying elements found in stainless steel, the iron in MS will oxidize quickly if not coated properly (Mora-Mendoza and Turgoose, 2002). This makes anti-corrosion coatings one of the most fruitful techniques for extending the life of MS used in applications ranging from transportation to infrastructure (Talo et al., 1999). Although the invention of effective coatings began with egg whites on the metal surface, today it has paved the way for the invention of intelligent and smart polymer and nanomaterials coatings (Montemor, 2014; Fayyad et al., 2016). The discovery of high-quality polymer nanocomposites is in high demand in this field with the main challenge being the invention of coatings that are less harmful to nature and with lucrative features (Nikpour et al., 2017; Mondal et al., 2015; Dong et al., 2018; Mirmohseni and Wallace, 2003). Sam John et al. synthesized chitosan/ZnO nanoparticle composite membranes for the enhancement of corrosion protection on mild steel (John et al., 2015). Jaseela et al. reported the development of flower-like hierarchical thiourea loaded titania–polyvinyl alcohol nanocomposite coatings for the corrosion protection of MS in hydrochloric acid (Jaseela and Joseph, 2018). K O Shamsheera et al. produces an enhanced anti-corrosion property of chitosan-based film on MS in different aggressive media using surface-modified SiO_2 (Shamsheera et al., 2020c). Therefore, this study focused on the usage of water-soluble polyvinyl alcohol (PVA) as a polymer material for the preparation of effective film-forming, non-toxic, and good adhesive quality polymer nanocomposites (Li et al., 2013). Here, graphene oxide (GO) is chosen as the most suitable filler for the polymer matrix because of its high barrier properties, high hydrophilic properties, and its ability to form layered films in water subjected to exfoliation (Kashyap et al., 2016). Furthermore, studies show that its structural features are effective in implementing GO-based polymer nanocomposites for maximum interfacial addition performance between the GO and the polymer matrix. The multi hydrogen bonds between the hydroxyl group of PVA and a variety of functional groups such as epoxides, carbonyls, hydroxyls, and phenyl groups attached to the surface of GO make a better polymer nanocomposite dispersion to generate flexibility, mechanical strength and express a large elongation at break and adopted as a better polymer nanocomposite material for this study than that of electrically conductive reduced graphene oxide as nanofiller (Rathod et al., 2016; Xu et al., 2009). Following Jiajie Liang et al. the preparation of a series of different wt% loading levels of GO in PVA using a simple water solution ultrasonication processing method is used (Liang et al., 2009). This allows good molecule-level dissemination of nanoparticles and also maximum interfacial interaction between the nanofiller and the polymer matrix (Gahlot et al.,

* Corresponding author.
E-mail address: abrahamjoseph@uoc.ac.in (A. Joseph).

https://doi.org/10.1016/j.rsurfi.2021.100018
Received 20 October 2020; Received in revised form 7 June 2021; Accepted 14 June 2021

2015). Non-electrochemical and electrochemical studies of PVA/GO in acidic and the saline medium was carried out to minimize the economic impact of corrosion to submarine pipelines, ships, and offshore drilling platforms, and so on (Mondal et al., 2015; Liu et al., 2003).

2. Experimental

For nanofiller synthesis, graphite flakes purchased from Sigma Aldrich, potassium permanganate ($KMnO_4$), sulfuric acid (H_2SO_4), and 30% H_2O_2 purchased from Merck chemicals were used. PVA (Art. 5315, LOBA CHEME PVT.LTD.) with molecular weight 115 kDa and degree of polymerization 1700–1800 are used for the formulation of the matrix. MS with an elemental composition (wt %): Fe (98.75%), C (0.20%), Mn (1%), P (0.03%), and S (0.02%) (EDAX technique) was selected as the test specimen for corrosion monitoring of finished coating metal products (Jaseela and Joseph, 2018). The electrochemical studies were directed using the MS coupons as a working electrode with an exposed area of 1 cm^2 to the corrosive environment. It is necessary to remove any extraneous soils, temporary protective films such as lacquer or grease from the finished surface by abrading using emery papers of grade 600–1200 with ethanol, acetone, and distilled water (ASTM standard G-1-72) for getting a water break-free surface. MS panels were dip coated into the PVA, GO, and various PVA/GO dispersions via the dip-coating method (SPEKTON dip coater). Cleaned and dried mild steel coupons were immersed into the solution for 20 s and withdrawn from it at a constant movement rate of 60 mm/min. After three consecutive dipping, the coated substrates were dried at room temperature for 24 h in the fume hood before corrosion study.

The aerated medium for the corrosion monitoring was obtained by the dilution of reagent grade HCl and NaCl using distilled water at atmospheric pressure and room temperature (Ammal et al., 2018). The electrochemical experiments were conducted in 0.5, 1, and 1.5 M HCl, and 3.5% NaCl as the corrosive media.

2.1. Fabrication of PVA/GO polymer nanocomposite

There have been many flourishing studies on how to build easily the GO nanoparticles. Here, we have selected the most effective Modified Hummer's method that has been proving through studies. In short; 1 g graphite flakes were mixed with 1 g of $NaNO_3$ followed by the addition of 25 ml con.H_2SO_4 in a 500 ml beaker maintained at an ice bath below 5 °C for 3 h. Then, 5 g of $KMnO_4$ was added to the above solution with vibrant stirring for the next 3 h. The resulting brownish blend was diluted by adding 100 ml deionized water and constantly stirred for further 2 h. Eventually, 20 ml of H_2O_2 (30%) was added slowly to the mixture to wind up the oxidation reaction until reaching an amber yellow color. The resulting mixture was centrifuged and washed with 5% HCl and distilled water to remove the superfluous ions. Then it was dried in a vacuum at 65 °C overnight. Exfoliated GO nanolayers in water can be obtained by mixing GO with water for 2 min by ultrasonication. 5.0% PVA solutions were prepared at 90 °C and through ultrasonication melded 1.0 weight % (wt%), 3.0 wt%, and 5.0 wt% GO dispersions into the viscous polymer matrices to obtain uniform dispersions (Dimiev and Tour, 2014; Krishnamoorthy et al., 2013; Marcano et al., 2010; Gao, 2015).

2.2. Surface characterization

The prepared PVA, GO and PVA/GO composites were characterized by using FTIR by KBr pellet method on a JASCO FTI-4100 instrument and electronic spectra by JASCO-UV–VIS 550 spectrophotometer. X-ray diffractograms of different films were recorded using the Rigaku Miniflex diffractometer. Atomic force microscopy (AFM) of the coated coupons was analyzed using Bruker multimode nanoscope version 8. ScanAsyst mode. FESEM analysis is used as an important supplement for the near-interaction microscopic studies of the polymer nanocomposite coated MS using Zeiss FESEM.

2.3. Corrosion monitoring

Long-term corrosion monitoring weight loss study helps to visually confirm the results and also the inspection of corrosion-induced damage to an object done by electrochemical methods like potentiodynamic polarization (PDP) and electrochemical impedance spectroscopy (EIS) through a series of surveys in a given period under identical conditions.

2.3.1. Electrochemical method

Since aqueous phased corrosions are electrochemical, electrochemical techniques like EIS and Tafel extrapolation methods were used to polarize the coated MS panels to accelerate the corrosion measurement process within 1 h. The current study was conducted with the help of a conventional 3 electrode corrosion measurement Gill AC computer-controlled electrochemical workstation (ACM instrument, model No: 1475). In which the coated and uncoated MS panels with 1 cm^2 area displayed for corrosion monitoring functions as a working electrode, a platinum foil act as a counter electrode, and a saturated calomel electrode (SCE) with a lugging capillary to reduce the IR drop act as a reference electrode. For better functioning, the working electrode was cleaned as per the ASTM-G-1-72 standard procedure and immersed in an electrolyte for attaining a stable quasi-steady-state potential. The EIS data processing was done by using Ziswimp Win Software (Shamsheera et al., 2020a).

2.3.1.1. Impedance spectroscopy (EIS). EIS is a non-destructive technique for the identification of even small rates of corrosion on a metallic body which cannot be evaluated by gravimetric methods. EIS deals with the collection of impedance data by perturbing the electrochemical system with an amplitude of 10 mV at a frequency range of 0.1 Hz to 10 KHz to give results as Nyquist and Bode plots by fitting the data with the help of different electrochemical circuits. EIS used for the assessment of η of a coating material using the equation,

$$\eta = \frac{R^*_{ct} - R_{ct}}{R^*_{ct}} \quad (1)$$

where R_{ct} and R^*_{ct} represent the charge transfer resistance in the uncoated and coated metals respectively obtained from fitted circuits (Shamsheera et al., 2020c,b).

2.3.1.2. Dynamic polarization (PDP) studies. In this voltage-regulated machinery, the three-electrode system is polarized by an overvoltage of 250 mV over a range of potentials from cathodic to anodic region with a scan rate of 1 mV/s. The current flowing through the cell in response to the generated electric field causes the electrode potential to be scanned at potentials above and below the E_{corr} leads to the determination of the kinetics of total anodic and cathodic processes respectively (Ko et al., 2019). Detecting passive behavior by increasing the applied anodic potential at constant current to plot Tafel lines to explore the parameters like the corrosion current density I_{corr}, corrosion potential E_{corr}, anodic and cathodic Tafel slopes β_a, and β_c, by Tafel extrapolation method. The η can be calculated from I_{corr} using this equation:

$$\eta = \frac{I^*_{corr} - I_{corr}}{I^*_{corr}} \quad (2)$$

where I^*_{corr} and I_{corr} are the corrosion current density of the uncoated and coated MS sample.

3. Result and discussion

3.1. Fourier transform infrared analysis (FTIR)

Fig. 1 displays the FTIR spectra of PVA, GO, and PVA/GO. GO nanoparticles enriched with a range of oxygenated functional groups on its hexagonal carbon framework were characterized by peaks at 1090 cm^{-1} (C–O), 1262 cm^{-1} (C–OH), 1750 cm^{-1} (C=O), 3432 cm^{-1}

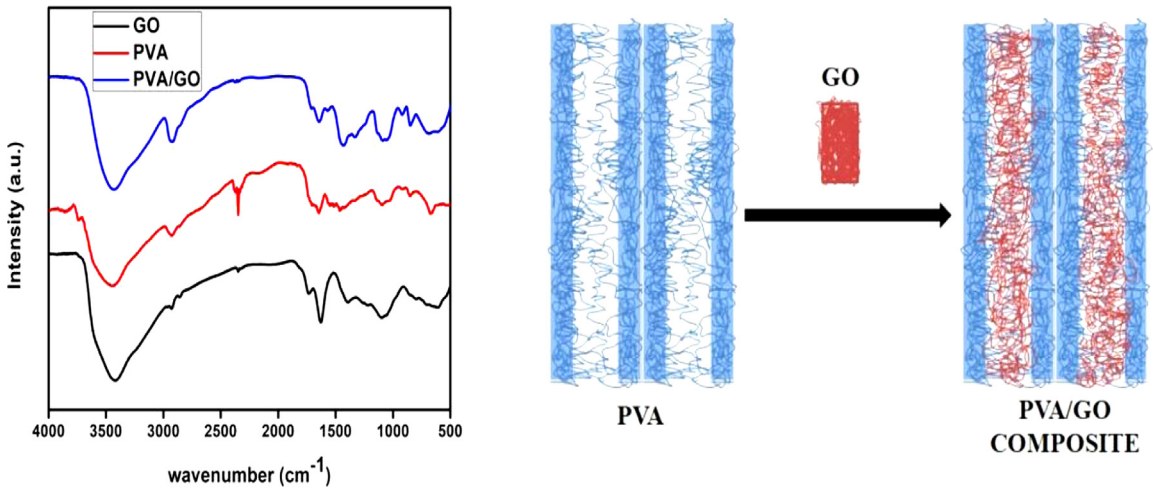

Fig. 1. FTIR spectra of GO, PVA and PVA/GO polymer nanocomposite and illustration of hydrogen bonding interaction between PVA and GO.

(O–H) and 920 cm^{-1} for epoxides (Bao et al., 2011; Chen et al., 2015). This unique structural feature manifests its greater polarity and granted excellent dissemination in the PVA matrix. PVA shows characteristic peaks at 3100–3600 cm^{-1} for ν_{O-H}, 2800–3000 cm^{-1}due to ν_{CH2} and 1000–1200 cm^{-1} for ν_{co} (Shao et al., 2016). For PVA/GO polymer nanocomposite, the shift in ν_{O-H} to smaller wave number shows the departure of hydrogen bonds between PVA molecules and its existence between PVA and GO molecules and which reveals a strong interfacial interaction between the polymer and the nanofiller. Most studies on PVA/GO composites refer to the reduction of H-bonds between PVA molecules as the "hydrogen-bond barrier effect" (Martin et al., 2018).

3.2. UV–visible spectroscopy

Fig. 2 correlates the optical measurements of exfoliated GO with that of the PVA /GO adhesive composite solution. Of the two peaks, one peak of GO at 232 nm, probably due to the π–π^* transition of the C–C double bonds of the hexagonal structure, and another shoulder peak at ~300 nm signifies the n-π^* transition of the carbonyl bonds (Chen et al., 2018). The absorption peak of the polymer nanocomposite film was in the same domicile of GO, which purports that PVA does not affect the absorption wavelength of GO.

3.3. X-ray diffraction (XRD) studies

XRD spectra peruse the dispersion quality of GO nanofillers in PVA polymer to establish the phase composition and microstructure of the polymer and nanoparticles. The 95 μm-thick (done by electronic screw gauge) PVA/3.0 wt% GO film with good flexibility and a surface free of roughness, bumps, or holes was subjected to this analysis (Xu et al., 2009). Chenlu Bao et al. proved that the XRD peak for graphite flakes is at $2\theta = 26.5°$ (Liu et al., 2016). But Fig. 3 discloses that the characteristic XRD peaks of pure GO sheets appeared at $2\theta = 9.4°$proportional to the d-spacing of 0.94 nm. From the literature review, it can be seen that the peak of PVA appeared at $2\theta = 19.5°$ (Yang and Lee, 2012). The XRD pattern of the PVA@3WGO films almost equivalent to that of the PVA diffraction peak, which is $2\theta = 19.27°$, and this value is mismatched with the characteristic diffraction peak of GO. This specifies that GO sheets were well exfoliated and uniformly dispersed in the PVA matrix (Aslam et al., 2019).

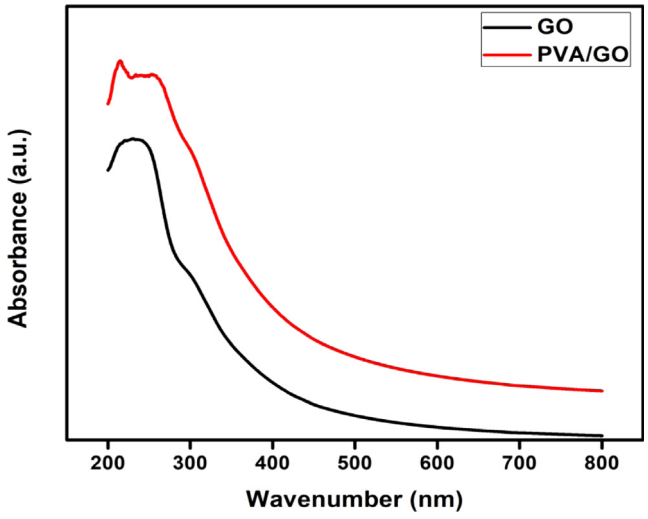

Fig. 2. UV–visible spectra of GO and PVA/GO solutions.

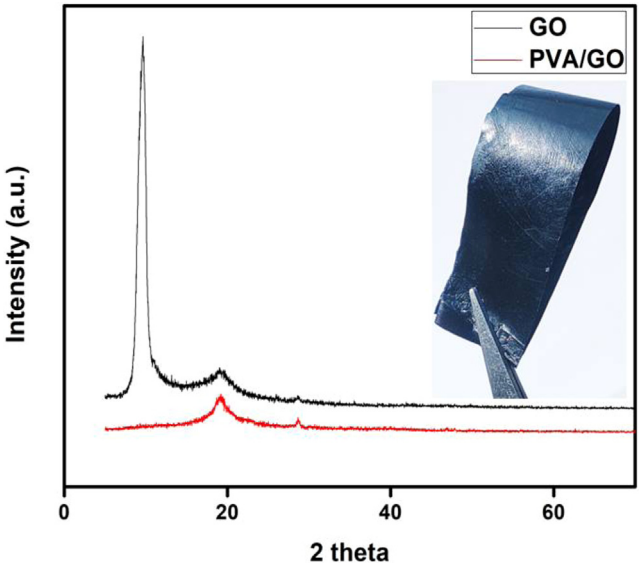

Fig. 3. XRD patterns of GO and PVA/GO composite and in inset, the photograph of a 95 μm-thick PVA/ GO composite film.

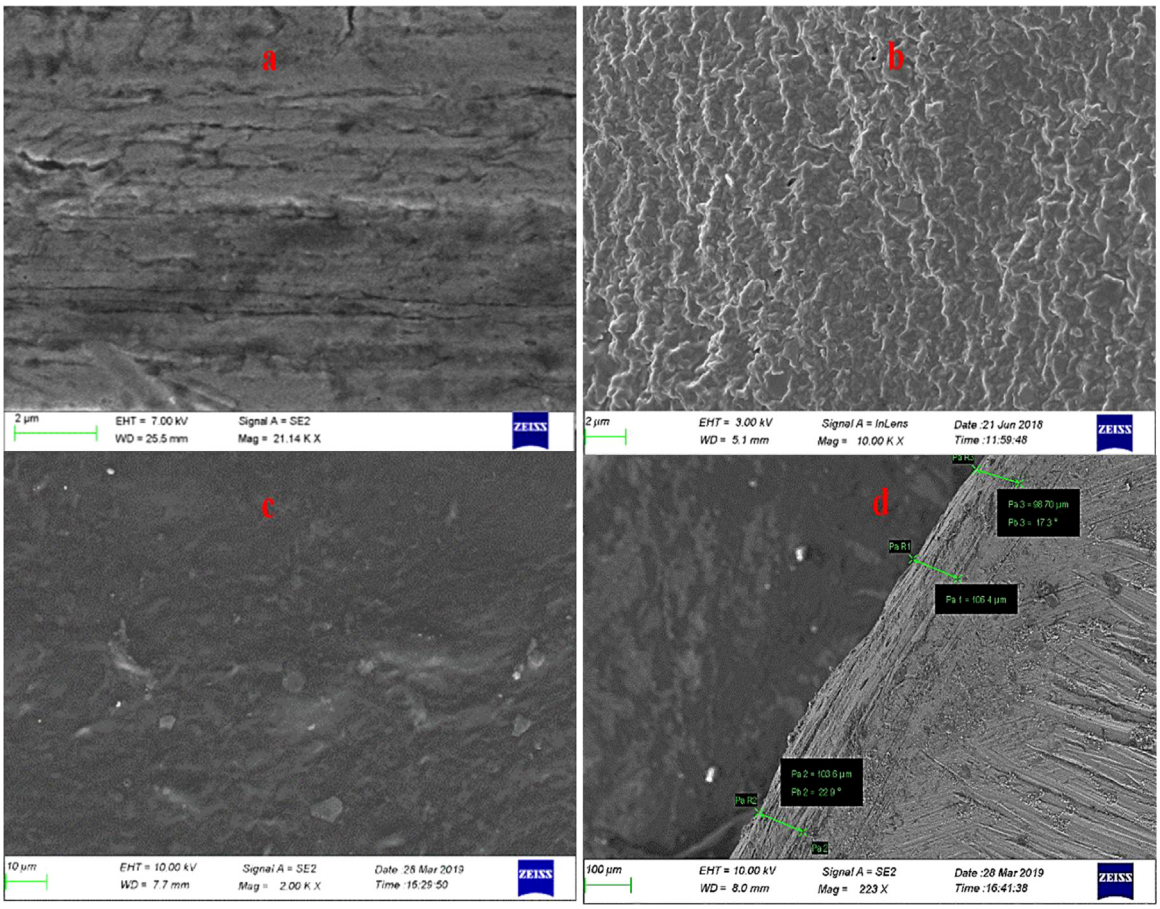

Fig. 4. FESEM image of (a) bare MS, (b) neat PVA, (c) PVA@3WGO, and (d) Cross-sectional image of PVA/GO on MS.

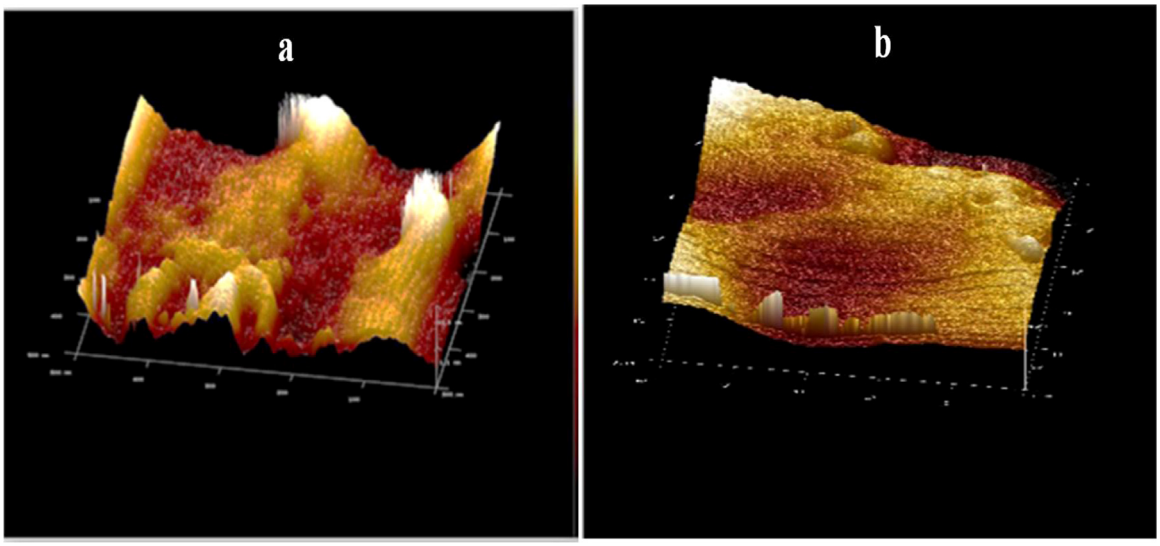

Fig. 5. AFM image of (a) PVA, and (b) PVA/3.0 wt% GO on MSMS.

3.4. FESEM and AFM

Compared with Fig. 4(a), (b) portrays the visual analysis of pure PVA coated MS using scanning electron microscopy makes clear that this continuous meshwork configuration of PVA is due to the presence of hydroxyl group on PVA (Yahia and Mohammed, 2018). The uniformity of the PVA/GO composite-covered surface on MS is shown in the Fig. 4(c) indicates that there is good compatibility between the polymer and nanofillers. This synergy between PVA and GO acts as a hermetic barrier against the penetration of corrosive species to reduce the degree of corrosion. From the cross-sectional FESEM image (Fig. 4(d)) the thickness of the PVA/GO uniform film coating on MS surface is around 102.9 µm. This is a topographical analysis that monitors the 3D portraying of PVA (Fig. 5(a)) and PVA/GO (Fig. 5(b)) coated surfaces to yield the values of R_a (average surface roughness) and R_q (root mean square surface roughness) (Zhang et al., 2014). The smaller R_a and R_q

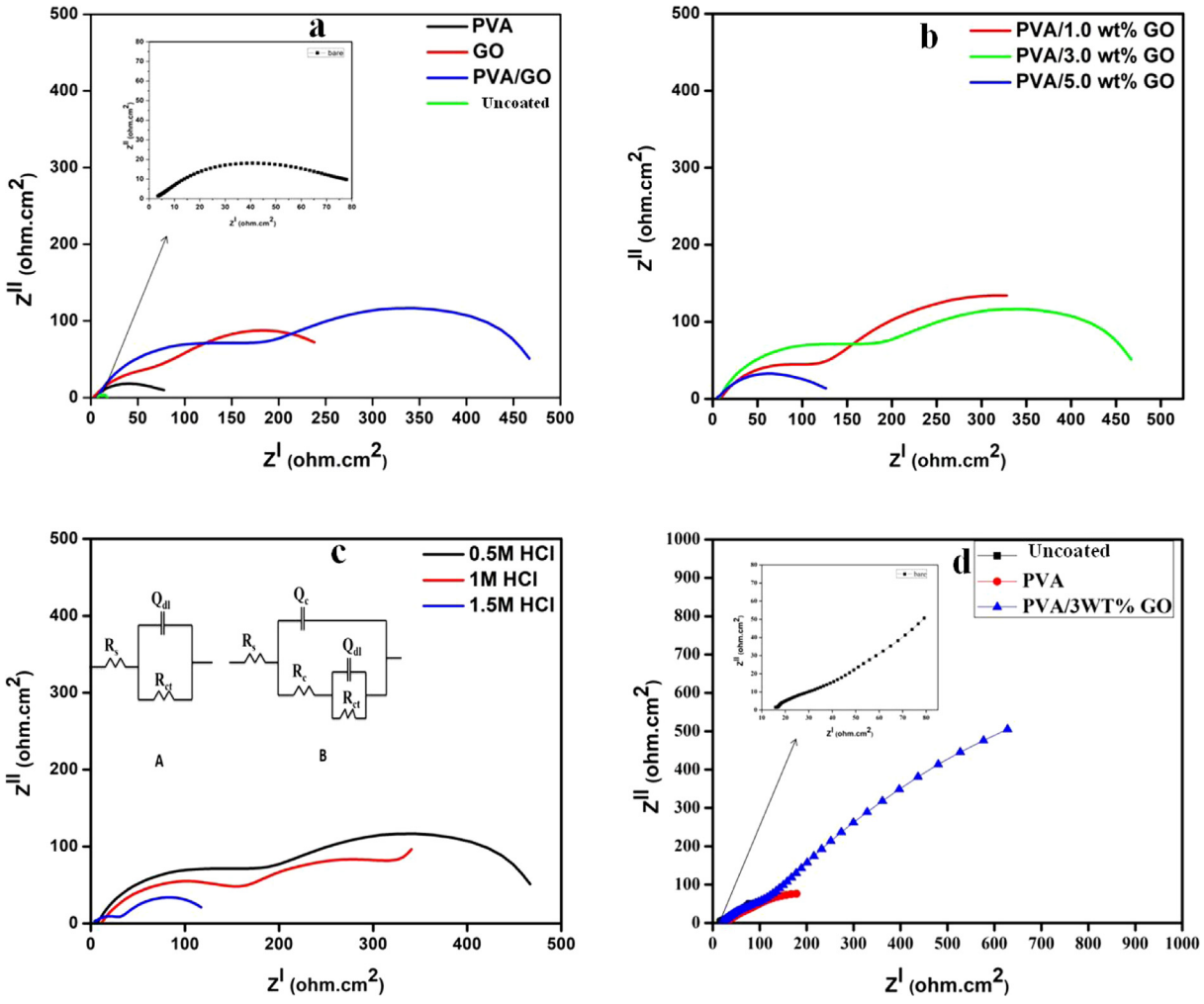

Fig. 6. Nyquist plots of (a) uncoated and coated MS in 0.5 M HCl, (b) various concentrations of GO in PVA, (c) PVA@3WGO in 0.5, 1 and 1.5 M HCl and in inset figure A and B are the preferred equivalent circuit model, and (d) uncoated and coated MS in 3.5% NaCl.

values f PVA/GO (R_a = 1.49 nm and R_q = 2.09 nm) than that of pure PVA (R_a = 1.95 nm and R_q = 2.51 nm) indicated that this polymer nanocomposite could form a uniform film coating on MS to act as a good anti-corrosive shield for the diffusion of different electrolyte. From this result, it can be concluded that PVA@3WGO acts as a better coating material than pure PVA.

3.5. Corrosion protection studies of PVA/GO nanocomposite film

3.5.1. Impedance analysis (EIS)

EIS responses are represented as Nyquist and Bode plots. The Nyquist plots for pure PVA, pure GO, and various concentrations of PVA/GO nanocomposites coated and uncoated MS after a stabilization period of 1 h in 0.5, 1, 1.5 M HCl, and 3.5% NaCl solutions are performed over a frequency range from 0.1 Hz to 10,000 Hz and are shown in Fig. 6. The experimental EIS data for uncoated samples, uncoated PVA are well fitted by the equivalent circuit R_s ($Q_{dl}R_{ct}$), whereas R_s ($Q_c(R_c(Q_{dl}R_{ct}))$) circuit gave the best fit for GO and PVA/GO polymer nanocomposites. The parameters used in the different circuits viz, R_s, R_{ct}, and R_c denote the electrolyte resistance, charge transfer resistance at metal electrolyte interface, and coating resistance at the electrolyte-coating interface, Q_{dl} and Q_c are the double-layer capacitance interface and coating capacitance at coating/electrolyte interface respectively. The impedance parameters obtained after data fittings are tabulated in Table 2. Fig. 6(a) displays the ameliorated impedance plot of PVA/GO compared to pure PVA and GO coated on MS in 0.5 M HCl in virtue of the good interfacial interaction between GO and PVA matrix. Moreover, the Q_c, coating capacitance, for PVA/3.0 wt% GO is lower than other coatings immersed in 0.5 M HCl on account of the filling of GO in the micropores of the polymer coating to abate the electrolyte uptake into the testing panel surface through the composite coating. Different weight percentage GO was loaded into the PVA matrix and it was observed that from the EIS plot (Fig. 6b), PVA@3WGO shows more protection efficiency (η = 97.8%) than other PVA/GO nanocomposite (η of PVA@1WGO = 96.7% & PVA@5WGO = 91). The lower η of 5.0 wt% GO in PVA polymer arises due to the GO–GO interactions rather than GO–PVA interaction. Fig. 6(c) exhibits an attractive feature of this polymer nanocomposite as a suitable corrosion defense material even in high concentrations of the acidic environment by showing good η values (η in1 M HCl = 96.4% & 1.5 M HCl = 92.6%). The PVA@3WGO shows its maximum efficiency in 0.5 M HCl rather than 1 and 1.5 M HCl solutions. In the EIS spectra of uncoated and PVA-coated MS, the one depressed semi-circle shows the charge transfer mechanism between the metal-electrolyte interface. When GO dispersed in the PVA, the Nyquist plot recorded two depressed semi-circles due to diffusion-controlled mechanisms (Niazi et al., 2015) which is also clear from the Bode plots. The impedance studies of 3.5% NaCl electrolyte indicate that PVA@3WGO has good resistance compared to bare PVA coated MS as shown by a significant increase in the diameter of the Nyquist plot (Fig. 6(d)). The high η of PVA@3WGO in the saline medium is attributed to the perfect thickness of PVA/GO coating which decreases the value of double-layer capacitance Q_{dl}, by the displacement of

Table 1
EIS parameters for uncoated and different coated MS systems.

Sample	Conc. of electrolyte	R_s (Ωcm^2)	Q_c ($S^n\Omega^{-1}cm^{-2}$)	n_1	R_c (Ωcm^2)	Q_{dl} ($S^n\Omega^{-1}cm^{-2}$)	n_2	R_{ct} (Ωcm^2)	PE (η)	Fitted circuit
Uncoated	0.5 M HCl	7.21	–	–	–	4.87×10^{-4}	0.80	10.34	–	A
PVA	0.5 M HCl	2.26	–	–	–	1.42×10^{-4}	0.80	80.19	87.1	A
GO	0.5 M HCl	2.50	1.47×10^{-3}	0.80	134.6	1.60×10^{-4}	0.91	173.30	94	B
PVA/1.0 wt% GO	0.5 M HCl	8.85	1.32×10^{-4}	0.70	143.4	1.07×10^{-4}	0.80	334.70	96.7	B
PVA/3.0 wt% GO	0.5 M HCl	6.68	1.06×10^{-4}	0.74	217.4	5.45×10^{-5}	0.87	477.70	97.8	B
PVA/5.0 wt% GO	0.5 M HCl	2.03	7.51×10^{-4}	0.50	129.2	7.76×10^{-5}	0.78	123.60	91.6	B
PVA/3.0 wt% GO	1 M HCl	11.54	1.06×10^{-4}	0.72	165.4	2.30×10^{-4}	0.73	247	96.4	B
PVA/3.0 wt% GO	1.5 M HCl	1.47	4.40×10^{-4}	0.56	37.8	2.80×10^{-3}	0.81	91.39	92.6	B
Uncoated	3.5% NaCl	11.92	–	–	–	2.90×10^{-4}	0.80	185.10	–	A
PVA	3.5% NaCl	25.59	–	–	–	2.62×10^{-4}	0.80	393.10	52.9	A
PVA/3.0 wt% GO	3.5% NaCl	18.99	7.11×10^{-4}	0.59	273.4	5.10×10^{-5}	0.80	1994	90.7	B

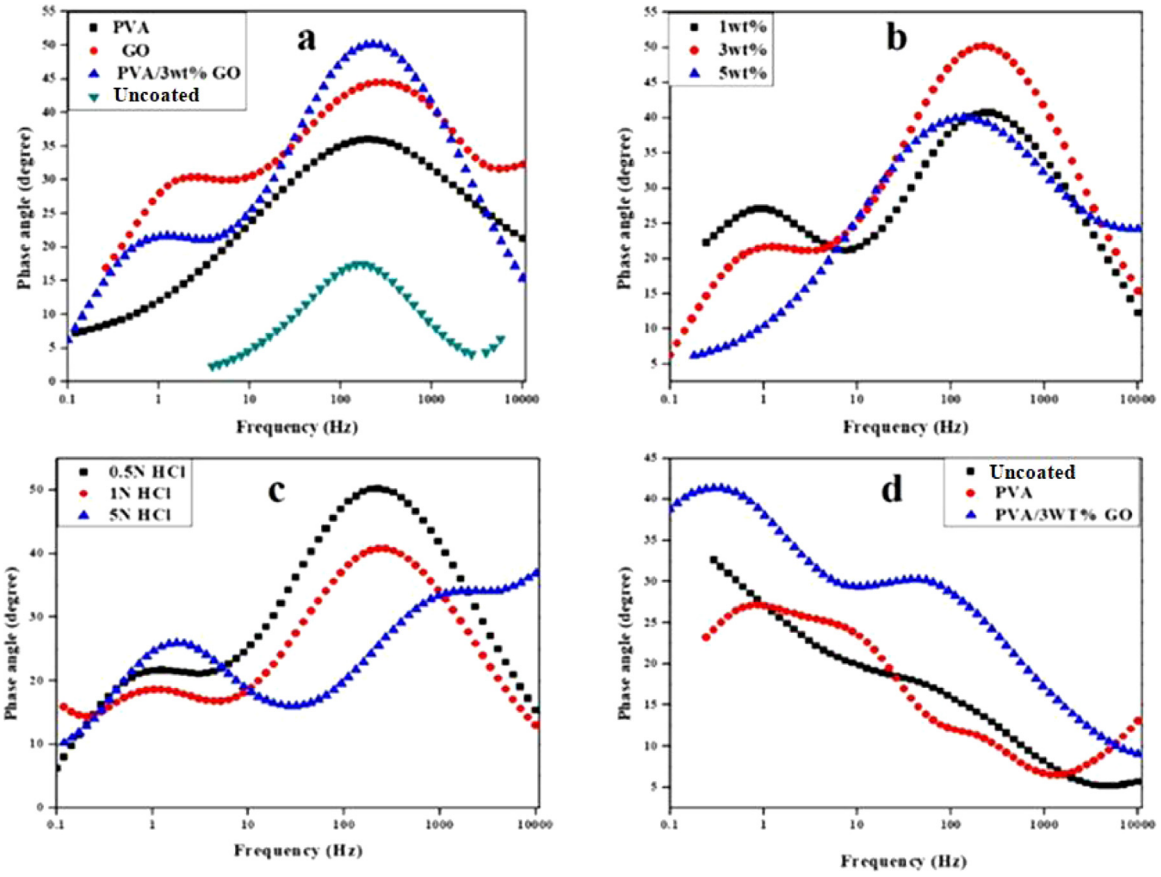

Fig. 7. Bode plots of (a) uncoated and coated MS in 0.5 M HCl, (b) various concentrations of GO in PVA, (c) PVA@3WGO in 0.5, 1 and 1.5 M HCl and (d) uncoated and coated ms in 3.5% NaCl.

water molecules and other ions adsorbed on the metal surface (El-Haddad, 2014). The results presented in Table 1 show that the R_{ct} values of coatings increase significantly by incorporating 3.0 wt% GO in PVA, which is supportive of the enhanced barrier properties of nanocomposite coatings (He et al., 2019). Meanwhile, the higher value of R_{ct} for PVA@3WGO can be explained by the good dispersibility of GO in coating and improving coating electrical resistance against the transfer of corrosive species through the pores of coating (Rikhari et al., 2018). Phase angle Vs frequency plots of pure PVA, GO and polymer nanocomposite coated and uncoated metal after immersion in various concentrations of HCl and 3.5% NaCl solution after a stabilization period of 1 h shown in Fig. 7. From Fig. 7 (a), we can see that the phase angle at high frequency for PVA/GO coating indicating strong interfacial interaction of nanocomposite coatings with the metal specimen (Carneiro et al., 2013). However, the results clearly show that the 3.0 wt% GO polymer nanocomposite coating remarkably influences the degree of corrosion protection of coatings compared to other GO concentrations.

3.5.2. Dynamic polarization study (PDP)

Tafel plots are obtained by extrapolating both cathodic and anodic linear regions back to the corrosion potential (E_{corr}) for uncoated and coated MS panels immersed in various concentrations of HCl and 3.5% NaCl solutions are shown in Fig. 8 and the corresponding corrosion parameters are codified in Table 2. The current investigation of coated and uncoated MS in 0.5 M HCl extended to other coating proportions and the values of corrosion rate (CR) are computed. The PVA@3WGO (41.87 mils per year) coating shows a much smaller value than uncoated MS, MS coated with pure PVA, pure GO, 1.0 wt%, and 5.0 wt% GO concentrations of polymer nanocomposites. The E_{corr} values of PVA, GO and PVA@3WGO in acidic solutions increase from −452.89 mV, −380.58 mV to −336.96 mV respectively. This flawless shift toward the positive region substantiates that PVA@3WGO polymer nanocomposite coated MS has resistance to corrosion in 0.5 M HCl. Polarization resistance, R_p, of the test species can be arrived at by using the Stern–Geary

Table 2
Potentiodynamic polarization parameters for corrosion of uncoated and coated samples in different electrolytic solutions.

Sample code	Conc.	E_{corr} (mV/SCE)	I_{corr} (mA/cm^2)	β_a (mV/dec)	β_c (mV/dec)	R_p (KΩcm^2)	CR (mm/year)	CR (mils/year)	PE%
Uncoated	0.5 M HCl	−462.50	1.2903	151.13	165.41	26.58	25.95	938.92	–
PVA	0.5 M HCl	−452.89	0.3361	95.29	164.50	77.95	18.15	714.79	85.45
GO	0.5 M HCl	−380.58	0.0908	105.70	204.34	333.14	2.41	94.81	96.06
PVA/1.0 wt% GO	0.5 M HCl	−472.18	0.2238	100.19	112.76	102.93	13.08	515.07	90.31
PVA/3.0 wt% GO	0.5 M HCl	−336.96	0.0450	108.91	167.68	637.09	1.06	41.87	98.05
PVA/5.0 wt% GO	0.5 M HCl	−461.42	0.2616	137.23	183.13	130.20	9.63	379.43	88.68
PVA/3.0 wt% GO	1 M HCl	−366.47	0.0913	172.79	239.63	477.48	1.85	72.57	75.63
PVA/3.0 wt% GO	1.5 M HCl	−401.92	0.3341	195.65	201.47	129	7.01	276.25	70.00
Uncoated	3.5% NaCl	−747.69	0.0316	78.23	221.35	794.31	2.72	56.12	–
PVA	3.5% NaCl	−759.19	0.0154	103.33	153.99	1743.84	1.42	55.78	51.26
PVA/3.0 wt% GO	3.5% NaCl	2172.9	0.0045	93.88	56.07	3387.27	0.08	3.21	85.76

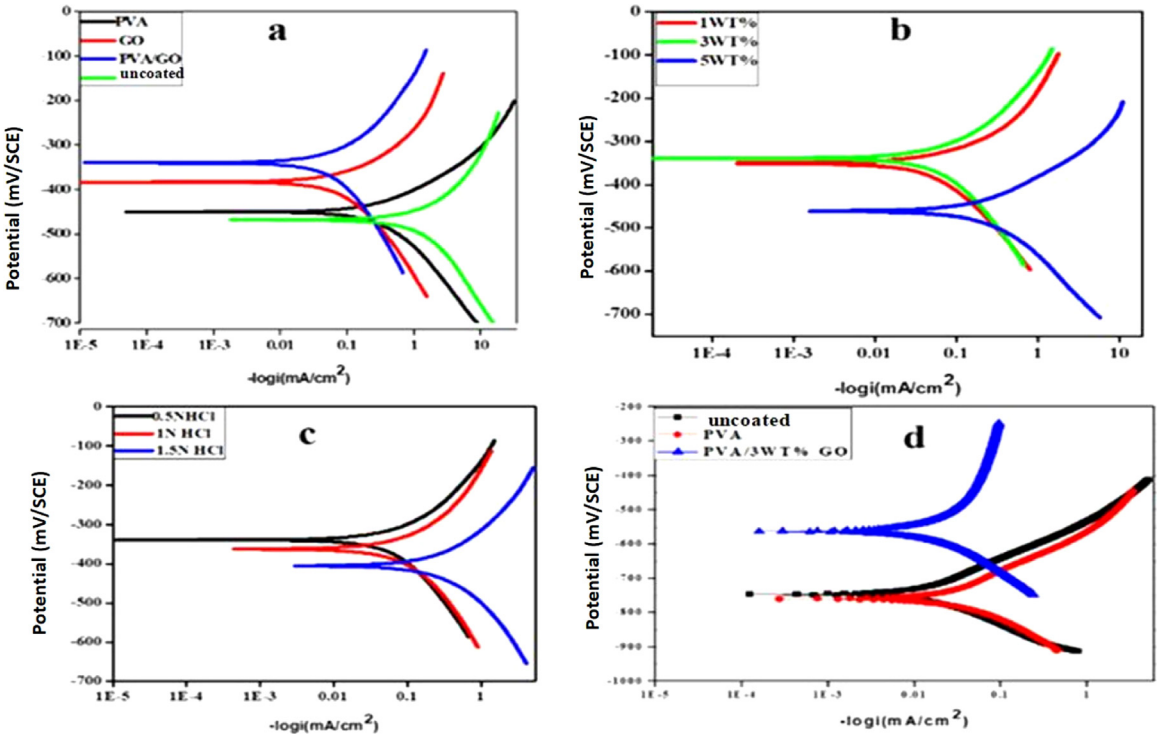

Fig. 8. Tafel plots of (a) uncoated and coated MS in 0.5 M HCl, (b) various concentrations of GO in PVA, and (c) PVA/3.0 wt% GO in 0.5, 1, and 1.5 M HCl, and (d) uncoated and coated MS in 3.5% NaCl.

equation,

$$R_p = \frac{\beta_a \beta_c}{2.303(\beta_a + \beta_c) I_{corr}} \quad (3)$$

where β_a and β_c as anodic and cathodic Tafel constants were determined from the extrapolation method. Among different loading levels of GO in PVA, I_{corr} is minimum for 3.0 wt% GO (0.0450 mA/cm^2) whereas I_{corr} is 0.2238 mA/cm^2 for 1.0 wt% GO and 0.2616 mA/cm^2 for 5.0 wt% GO. These results indicate that 3.0 wt% GO fillers enhance the corrosion protection ability of the PVA-coated system to defend against corrosion. When 3.0 wt% GO as filler dispersed into the PVA matrix, PVA@3WGO composite coating containing two different materials and enjoying the combined properties act as a hedge to block the diffusion of corrosive substances. Therefore, it is effective for MS protection. The increase in polarization resistance (R_p = 3382.7 KΩcm^2) further confirms the enhanced resistance of PVA@3WGO coated MS and a lower I_{corr} and CR indicate better corrosion protection properties. The PDP studies conducted in 3.5% NaCl provide parameters that reached the expected range and give good results compared to the EIS data. From Fig. 8(d) and Table 2, it can be seen that the I_{corr} and R_p values of uncoated MS sample in 3.5% NaCl solution were found to be 0.0316 mA/cm^2 and 794.31 KΩcm ^{2} respectively. However, when the MS panel was coated with pure PVA, the I_{corr} values decreased to 0.0154 mA/cm^2, and the R_p values increased, which is approximately 2 times lower than that of the uncoated steel sample. When the MS panel was coated with PVA@3WGO composite coating, the I_{corr} value decreased to 0.0045 mA/cm^2, while the R_p value increased to 3387.27 KΩcm^2. The increased R_p value is mainly due to the decreased diffusion of hydrogen cations, chloride ions, water molecules, etc. into the test panel surface from the electrolyte. This study indicates direct proportionality between I_{corr} value and acid concentration while the inverse proportionality between R_p and concentration of acidic medium is the corrosive environment (Feliu et al., 1998). From the PDP data, the PE values of the pure PVA coating and PVA@3WGO composite coating in an alkaline medium are about 51.26% and 85.76%, respectively. These results reveal that PVA@3WGO composite coating effectively protects the MS and improves the corrosion protection efficiency.

4. Conclusions

- FTIR, UV–Visible spectra and the XRD analysis certifies the good dispersion and exfoliation of nanofiller in the water-based polymer.

- Surface monitoring by SEM and AFM shows that PVA@3WGO is a suitable homogeneous corrosion-resistant film for MS and its prolonged protection in acid and saline environments can be ensured.
- Impedance results indicate that PVA@3WGO has higher η (97.8%) and R_{ct} (477.70 Ωcm^2) as compared to other coated substrates in 0.5 M HCl than in 1 M and 1.5 M HCl.
- Bode plots also support these results by giving a phase angle at high frequency for PVA/3.0 wt% GO composite coated on MS which substantiate the fact that it acts as one of the best coating materials in acidic and alkaline solutions.
- The increased polarization resistance both in 0.5 M HCl (637.09 $K\Omega cm^2$) and 3.5% NaCl (3387.27 $K\Omega cm^2$) and decreased I_{corr} (0.0450 mA/cm^2 in 0.5 M HCl and 0.0045 mA/cm^2 in 3.5% NaCl) of composite coated MS was measured from PDP studies.
- Both EIS and PDP studies show that the η of the various concentrations of GO as filler in PVA coating is followed: 5.0 wt% Go < 1.0 wt% GO < 3.0 wt% GO.

Declaration of competing interest

The authors declare that they have no known competing financial interests or personal relationships that could have appeared to influence the work reported in this paper.

Acknowledgments

Anila Paul, and Anupama R Prasad acknowledge the financial support given by University of Calicut, India and Shamsheera K O acknowledge University Grants Commission (UGC), Government of India for providing financial support in the form of research fellowship. The authors also acknowledge the service received from DST-FIST facility, Department of Chemistry and CSIF University of Calicut.

References

Ammal, P.R., Prajila, M., Joseph, A., 2018. Effect of substitution and temperature on the corrosion inhibition properties of benzimidazole bearing 1, 3, 4-oxadiazoles for mild steel in sulphuric acid: Physicochemical and theoretical studies. J. Environ. Chem. Eng. 6, 1072–1085.

Aslam, M., Kalyar, M.A., Raza, Z.A., 2019. Investigation of structural and thermal properties of distinct nanofillers-doped PVA composite films. Polym. Bull. 76, 73–86.

Bao, C., Guo, Y., Song, L., Hu, Y., 2011. Poly (vinyl alcohol) nanocomposites based on graphene and graphite oxide: A comparative investigation of property and mechanism. J. Mater. Chem. 21, 13942–13950.

Carneiro, J., Tedim, J., Fernandes, S.C., Freire, C., Gandini, A., Ferreira, M., Zheludkevich, M., 2013. Functionalized chitosan-based coatings for active corrosion protection. Surf. Coat. Technol. 226, 51–59.

Chen, J., Li, Y., Zhang, Y., Zhu, Y., 2015. Preparation and characterization of graphene oxide reinforced PVA film with boric acid as a crosslinker. J. Appl. Polym. Sci. 132.

Chen, W., Liu, P., Min, L., Zhou, Y., Liu, Y., Wang, Q., Duan, W., 2018. Non-covalently functionalized graphene oxide-based coating to enhance thermal stability and flame retardancy of PVA film. Nano-Micro Lett. 10, 39.

Dimiev, A.M., Tour, J.M., 2014. Mechanism of graphene oxide formation. ACS Nano 8, 3060–3068.

Dong, Y., Li, S., Zhou, Q., 2018. Self-healing capability of inhibitor-encapsulating polyvinyl alcohol/polyvinylidene fluoride coaxial nanofibers loaded in epoxy resin coatings. Prog. Org. Coat. 120, 49–57.

El-Haddad, M.N., 2014. Hydroxyethylcellulose used as an eco-friendly inhibitor for 1018 c-steel corrosion in 3.5% NaCl solution. Carbohydr. Polymers 112, 595–602.

Fayyad, E.M., Sadasivuni, K.K., Ponnamma, D., Al-Maadeed, M.A.A., 2016. Oleic acid-grafted chitosan/graphene oxide composite coating for corrosion protection of carbon steel. Carbohydr. Polymers 151, 871–878.

Feliu, V., González, J., Adrade, C., Feliu, S., 1998. Equivalent circuit for modelling the steel-concrete interface. II. Complications in applying the Stern-Geary equation to corrosion rate determinations. Corros. Sci. 40, 995–1006.

Gahlot, S., Kulshrestha, V., Agarwal, G., Jha, P.K., 2015. Synthesis and characterization of PVA/GO nanocomposite films. In: Macromolecular Symposia. Wiley Online Library, pp. 173–177.

Gao, W., 2015. The chemistry of graphene oxide. In: Graphene Oxide. Springer, pp. 61–95.

He, Y., Boluk, Y., Pan, J., Ahniyaz, A., Deltin, T., Claesson, P.M., 2019. Corrosion protective properties of cellulose nanocrystals reinforced waterborne acrylate-based composite coating. Corros. Sci. 155, 186–194.

Jaseela, P., Joseph, A., 2018. Development of flower like hierarchical thiourea loaded titania–poly vinyl alcohol nano composite coatings for the corrosion protection of mild steel in hydrochloric acid. J. Inorg. Organomet. Polym. Mater. 28, 1468–1482.

John, S., Joseph, A., Jose, A.J., Narayana, B., 2015. Enhancement of corrosion protection of mild steel by chitosan/ZnO nanoparticle composite membranes. Prog. Org. Coat. 84, 28–34.

Kashyap, S., Pratihar, S.K., Behera, S.K., 2016. Strong, and ductile graphene oxide reinforced PVA nanocomposites. J. Alloys Compd. 684, 254–260.

Ko, S., Prasad, A.R., Garvasis, J., Basheer, S.M., Joseph, A., 2019. Stearic acid grafted chitosan/epoxy blend surface coating for prolonged protection of mild steel in a saline environment. J. Adhes. Sci. Technol. 33, 2250–2264.

Krishnamoorthy, K., Veerapandian, M., Yun, K., Kim, S.-J., 2013. The chemical and structural analysis of graphene oxide with different degrees of oxidation. Carbon 53, 38–49.

Kroon, D.H., Bowman, E., Jacobson, G., 2019. Corrosion management can save water and wastewater utility billions of dollars annually. J. Am. Water Works Assoc. 111.

Li, Y., Umer, R., Samad, Y.A., Zheng, L., Liao, K., 2013. The effect of the ultrasonication pre-treatment of graphene oxide (GO) on the mechanical properties of GO/polyvinyl alcohol composites. Carbon 55, 321–327.

Liang, J., Huang, Y., Zhang, L., Wang, Y., Ma, Y., Guo, T., Chen, Y., 2009. Molecular-level dispersion of graphene into poly (vinyl alcohol) and effective reinforcement of their nanocomposites. Adv. Funct. Mater. 19, 2297–2302.

Liu, H., Bandyopadhyay, P., Kim, N.H., Moon, B., Lee, J.H., 2016. Surface modified graphene oxide/poly (vinyl alcohol) composite for enhanced hydrogen gas barrier film. Polym. Test. 50, 49–56.

Liu, C., Bi, Q., Leyland, A., Matthews, A., 2003. An electrochemical impedance spectroscopy study of the corrosion behavior of PVD coated steels in 0.5 N NaCl aqueous solution: Part II.: EIS interpretation of corrosion behavior. Corros. Sci. 45, 1257–1273.

Marcano, D.C., Kosynkin, D.V., Berlin, J.M., Sinitskii, A., Sun, Z., Slesarev, A., Alemany, L.B., Lu, W., Tour, J.M., 2010. Improved synthesis of graphene oxide. ACS Nano 4, 4806–4814.

Martin, M., Prasad, N., Sivalingam, M.M., Sastikumar, D., Karthikeyan, B., 2018. Optical, phonon properties of ZnO–PVA, ZnO–GO–PVA nanocomposite free-standing polymer films for UV sensing. J. Mater. Sci., Mater. Electron. 29, 365–373.

Mirmohseni, A., Wallace, G., 2003. Preparation and characterization of processable electroactive polyaniline–polyvinyl alcohol composite. Polymer 44, 3523–3528.

Mondal, J., Kozlova, M., Sammelselg, V., 2015. Graphene nanoplatelets based protective and functionalizing coating for stainless steel. J. Nanosci. Nanotechnol. 15, 6747–6750.

Montemor, M., 2014. Functional and smart coatings for corrosion protection: A review of recent advances. Surf. Coat. Technol. 258, 17–37.

Mora-Mendoza, J., Turgoose, S., 2002. Fe_3C Influence on the corrosion rate of mild steel in aqueous CO_2 systems under turbulent flow conditions. Corros. Sci. 44, 1223–1246.

Niazi, M.R., Li, R., Li, E.Q., Kirmani, A.R., Abdelsamie, M., Wang, Q., Pan, W., Payne, M.M., Anthony, J.E., Smilgies, D.-M., 2015. Solution-printed organic semiconductor blends exhibiting transport properties on par with single crystals. Nature Commun. 6, 1–10.

Nikpour, B., Ramezanzadeh, B., Bahlakeh, G., Mahdavian, M., 2017. Synthesis of graphene oxide nanosheets functionalized by green corrosion inhibitive compounds to fabricate a protective system. Corros. Sci. 127, 240–259.

Rathod, S.G., Bhajantri, R., Ravindrachary, V., Naik, J., Kumar, D.M., 2016. High mechanical and pressure-sensitive dielectric properties of graphene oxide doped PVA nanocomposites. RSC Adv. 6, 77977–77986.

Rikhari, B., Mani, S.P., Rajendran, N., 2018. Electrochemical behavior of polypyrrole/chitosan composite coating on Ti metal for biomedical applications. Carbohydr. Polymers 189, 126–137.

Shamsheera, K., Anupama, R.P., Abraham, J., 2020a. Computational simulation, surface characterization, adsorption studies and electrochemical investigation on the interaction of guar gum with mild steel in HCl environment. Results Chem. 100054.

Shamsheera, K., Prasad, A.R., Jaseela, P., Joseph, A., 2020b. Development of self-assembled monolayer of stearic acid grafted chitosan on mild steel and inhibition of corrosion in hydrochloric acid. Chem. Data Collect. 100402.

Shamsheera, K., Prasad, A.R., Joseph, A., 2020c. Extended protection of mild steel in saline and acidic environment using stearic acid grafted chitosan preloaded with mesoporous-hydrophobic silica ($mhSiO_2$). Surf. Coat. Technol. 126350.

Shao, L., Li, J., Guang, Y., Zhang, Y., Zhang, H., Che, X., Wang, Y., 2016. PVA/polyethyleneimine-functionalized graphene composites with optimized properties. Mater. Des. 99, 235–242.

Talo, A., Forsen, O., Yläsaari, S., 1999. Corrosion protective polyaniline epoxy blend coatings on mild steel. Synth. Met. 102, 1394–1395.

Xu, Y., Hong, W., Bai, H., Li, C., Shi, G., 2009. Strong and ductile poly (vinyl alcohol)/graphene oxide composite films with a layered structure. Carbon 47, 3538–3543.

Yahia, I., Mohammed, M., 2018. Facile synthesis of graphene oxide/PVA nanocomposites for laser optical limiting: Bandgap analysis and dielectric constants. J. Mater. Sci., Mater. Electron. 29, 8555–8563.

Yang, J.-H., Lee, Y.-D., 2012. Highly electrically conductive rGO/PVA composites with a network dispersive nanostructure. J. Mater. Chem. 22, 8512–8517.

Zhang, J., Wang, J., Lin, T., Wang, C.H., Ghorbani, K., Fang, J., Wang, X., 2014. Magnetic and mechanical properties of polyvinyl alcohol (PVA) nanocomposites with hybrid nanofillers–graphene oxide tethered with magnetic Fe_3O_4 nanoparticles. Chem. Eng. J. 237, 462–468.